The Performance of Hydrological Monthly Products Using SSM/I–SSMI/S Sensors

DANIEL VILA

*Centro de Previsão do Tempo e Estudos Climaticos, Instituto Nacional de Pesquisas Espacias, Cachoeira Paulista, Brazil,
and Cooperative Institute of Climate Studies, College Park, Maryland*

CECILIA HERNANDEZ

Cooperative Institute of Climate Studies, College Park, Maryland

RALPH FERRARO

Cooperative Institute of Climate Studies, College Park, and NOAA/NESDIS, Silver Spring, Maryland

HILAWE SEMUNEGUS

NCDC/NOAA, Asheville, North Carolina

(Manuscript received 17 April 2012, in final form 11 June 2012)

ABSTRACT

Global monthly rainfall estimates and other hydrological products have been produced from 1987 to the present using measurements from the Defense Meteorological Satellite Program (DMSP) series of the Special Sensor Microwave Imager (SSM/I). The aim of this paper is twofold: to present the recent efforts to improve the quality control (QC) of historical antenna temperature of the SSM/I sensor (1987–2008) and how this improvement impacts the different hydrological products that are generated at NOAA/National Environmental Satellite, Data, and Information Service (NESDIS). Beginning in 2005, the DMSP Special Sensor Microwave Imager/Sounder (SSMI/S) has been successfully operating on the *F-16*, *F-17*, and *F-18* satellites. The second objective of this paper is focused on the application of SSMI/S channels to evaluate the performance of several hydrological products using the heritage of existing SSM/I algorithms and to develop an improved strategy to extend the SSM/I time series into the SSMI/S era, starting with data in 2009 for *F-17*. The continuity of hydrological products from SSM/I to SSMI/S has shown to be a valuable contribution for the precipitation and climate monitoring community but several sensor issues must be accounted for to meet this objective.

1. Introduction

Global monthly rainfall estimates and other hydrological products like integrated liquid water path (LWP) and total precipitable water (WVP) have been produced from 1987 to present using measurements from the Defense Meteorological Satellite Program (DMSP) series of the Special Sensor Microwave Imager (SSM/I). The DMSP *F-16* satellite was successfully launched on 18 October 2003, carrying on board the first Special Sensor Microwave Imager/Sounder (SSMI/S) followed by DMSP *F-17* and *F-18* launched in 2009 and 2010, respectively. The SSMI/S are the first operational microwave satellite radiometers for profiling temperature and humidity using a conical scanning sensor, so that the viewing area and slant path remains constant as it scans Earth (Poe et al. 2001). SSMI/S imaging channels maintain similar resolution and spectral frequency to the SSM/I except 91.655 GHz on SSMI/S versus 85.5 GHz on SSM/I. Additionally, the SSMI/S added a new 150-GHz channel plus three humidity profiling channels, which consist of pairs of narrow passbands on either side of the H_2O absorption line center at 183.3 GHz similar to those on the Advanced Microwave Sounding Unit-B/Microwave Humidity Sounder (AMSU-B/MHS) instruments. A wider swath, approximately 1700 km for

Corresponding author address: Daniel Vila, Centro de Previsão do Tempo e Estudos Climaticos, Instituto Nacional de Pesquisas Espacias, Aut. Pres. Dutra KM 40, Cachoeira Paulista, SP, CEP 12 630-000, Brazil.
E-mail: daniel.vila@cptec.inpe.br

SSMI/S compared with only 1400 km for SSM/I, is also a new characteristic of this instrument. Two more SSMI/S sensors are anticipated on the *F-19* and *F-20* satellites to be launched later this decade.

This research has two objectives: the reprocessing of the existing SSM/I database using an improved quality control (QC) scheme for antenna temperatures (Vila et al. 2010) for the entire period 1987–2009 and the continuation in monitoring and retrieving of atmospheric and surface parameters such as precipitation (Ferraro 1997), sea ice, and liquid water path (Alihouse et al. 1990), among other products using SSMI/S measurements.

These products, combined with those derived from other passive microwave sensors such as AMSU/MHS on board National Oceanic and Atmospheric Administration (NOAA) satellites, offer the scientific community an excellent source of global hydrological products. The high temporal frequency of rainfall retrievals and other hydrological products will also help to better understand the diurnal cycle for different climate regimes around the world (Vila et al. 2007).

This paper is organized as follows: In section 2 a brief description of the algorithms, the data used in this research, and a brief description of the improved QC scheme for SSM/I are presented. The brightness temperature calibration methodology for SSMI/S using a histogram matching technique will be discussed in section 3. Time series analysis and some comparisons between SSM/I *F-13* and SSMI/S *F-17* products will be presented in section 4, while section 5 is focused on the conclusion and the follow-on research.

2. Data and algorithms

a. Data sources

For this particular project, SSM/I and SSMI/S temperature data record (TDR) files from the Comprehensive Large Array-Data Stewardship System (CLASS) were used. CLASS is a web-based data archive and distribution system for NOAA's environmental data. TDRs contain calibrated and earth-located data prior to irreversible antenna pattern correction. The temperature data represent microwave energy levels measured by the radiometer instrument. The energy levels are expressed as an equivalent backbody temperature [antenna temperature (AT)]. This file also contains information about surface type, rain flag (in case of SSMI/S), and scan number position. Nevertheless, the file structure for both satellites is different, because of the geometry and the number of feedhorns in each platform. More information about SSM/I and SSMI/S TDR files used in this study can be found in the NOAA National Climatic Data Center

web page (http://www.ncdc.noaa.gov/oa/rsad/ssmi/ssmi.html). These files have been mapped to $1/3°$ latitude $\times$ $1/3°$ longitude linear daily grids for the ascending and descending nodes, respectively. This method was established in the early stages of the Global Precipitation Climatology Project (GPCP) and must be maintained for continuity of the GPCP V2 global rainfall products; however, it is recognized that a superior product could be developed using the highest-resolution data. For this study, we have used all available data from *F-08*, *F-10*, *F-11*, *F-13*, *F-14*, and *F-15* satellites. *F-08* data treatment will be discussed in the next section. In the case of *F-16*, *F-17*, and *F-18*, only seven channels were remapped to daily grids to match with the correspondent channels of SSM/I sensor. SSMI/S imaging channels maintain similar resolution and spectral frequency to the SSM/I except 91.655 GHz on SSMI/S versus 85.5 GHz on SSM/I as was mentioned in the introduction.

To evaluate how the QC scheme could affect precipitation products, three precipitation product were used: 1) the GPCP (Huffman et al. 2009), which is a product obtained by optimally merging estimates computed from microwave, infrared, and sounder data and precipitation gauge analyses; 2) the Global Precipitation Climatology Centre (GPCC; Rudolf 1993) based on rain gauge analysis only; and 3) NOAA's Precipitation Reconstruction over Land (PREC/L; Chen et al. 2002), which is also based on rain gauges observations from the Global Historical Climatology Network (GHCN), version 2, and the Climate Anomaly Monitoring System (CAMS) datasets.

b. Algorithms

A scattering-based rainfall algorithm is used to create the global rainfall estimates originating from the 85.5 GHz "scattering index" (SI) approach developed by Grody (1991). The final version of this algorithm is fully described in Ferraro (1997, his appendix A). This version also includes an emission-based component over ocean based on the LWP algorithm of Weng and Grody (1994). This algorithm was originally developed for SSM/I sensors and has been successfully incorporated in many well-known projects like GPCP, which consists of global monthly, 2.5° latitude–longitude averages (Huffman et al. 2009). An alternative version of this algorithm uses 37 GHz for the scattering approach. This version became very useful during the period when the high-frequency channel (85.5 GHz) on *F-08* failed.

Over the ocean, two other hydrological variables were tested: WVP and LWP. The retrieval of WVP is based on previous studies carried out by Alihouse et al. (1990) and updated by Ferraro et al. (1996). This variable is retrieved only under nonrain conditions over the ocean

using a quadratic regression of all vertical polarization SSM/I brightness temperature channels (excluding 85.5 GHz) regressed against the TPW determined with rawinsondes. The TPW algorithm includes a cubic correction of the WVP in low- and high-WVP regimes (see Colton and Poe 1994). Cloud liquid water path (CLW) retrieval is based on an emission-based algorithm proposed by Weng and Grody (1994). In this case, liquid water estimates based on 19, 37, and 85 GHz are valid over different ranges of liquid water content.

c. Improved QC methodology

The improved QC scheme is based on the detection of outliers for each grid box and every channel on the remapped antenna temperature files. This procedure was performed based on standardized temperature that uses the mean (μ) and standard deviation (σ) in each grid box for the period 1992–2007. The process to remove unrealistic values is based on the distance (in terms of standard deviation units) between the observed temperature and the mean value. If, for a given location, at least one channel is beyond 10 times the standard deviation from the mean value, then these data are flagged. After applying this process, it was found that not all spurious values are removed from the database. In those regions with large variability, 10 times the standard deviation leads to very high or very low physically inconsistent boundaries that cannot be used to remove suspicious values. In this case, a maximum and a minimum temperature threshold are set to 325 and 70 K, respectively, and all data beyond those limits are also flagged. The last QC constrain is related with the fact that, for a given grid point, the same failure is frequently observed in more than one channel. If the observed value of four or more channels is beyond 6 times the standard deviation from the mean value, that grid point is also flagged. All the grid points flagged in any of the three steps described above were not considered for retrieving the hydrological variables. For detailed information about the QC procedures see Vila et al. (2010).

It is important to mention that during the first stages of the SSM/I series (August 1987–December 1991) only *F-08* was flying and that period was not considered in the previous study because during the period of June 1990– December 1991, the 85-GHz channels aboard SSM/I *F-8* failed, so it was not possible to use the proposed algorithms. On the other hand, the daily grids files were in a different spatial scale, so it wasn't possible to apply the proposed QC scheme.

For this particular research, and because one of the goals of this study is to get the complete database for those variables that are not using 85 GHz, the early stages of the SSM/I series (August 1987–December
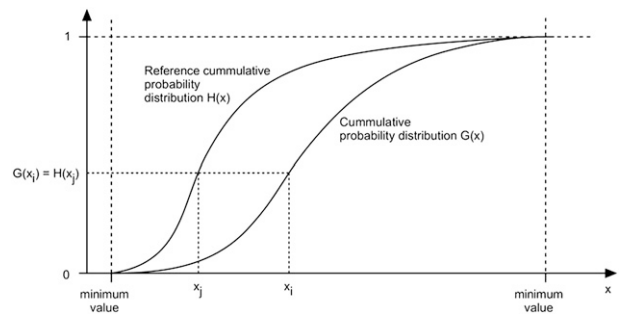

FIG. 1. Schematic representation of the histogram matching technique (adapted from http://paulbourke.net/texture_colour/equalisation/).

1991) were reprocessed from original swath files to $\frac{1}{3}°$ latitude × $\frac{1}{3}°$ longitude linear daily grids for the ascending and descending nodes, respectively, and the QC scheme was applied as described in the previous paragraph. In the period of June 1990–December 1991, the last constrain was not applied because only five channels are available.

For the period of missing data for 85 GHz, only two variables were computed: rain rate (37-GHz V scattering index algorithm; Ferraro 1997) and sea ice. In the case of rain rate, in order to get continuous sampling along the time with no gaps, the time series using the original 85-GHz algorithm was merged with the 37-GHz algorithm retrievals (37 GHz) for the period of missing data for 85 GHz (June 1990–December 1991).

3. The histogram matching approach

Histogram matching is a process where a time series, image, or higher-dimension scalar data (SSMI/S brightness temperature) is modified such that its histogram matches that of another reference dataset (SSM/I brightness temperature, in this case) (Gonzalez and Woods 2002). In this particular application, seven channels of the SSM/I sensor were "matched" with the correspondent channels in the SSMI/S array.

The algorithm is as follows. The cumulative histogram is computed for each dataset (see Fig. 1). For any particular value (x_i) in the data that has to be adjusted, there is a cumulative histogram value given by $G(x_i)$. This in turn is the cumulative distribution value in the reference dataset, namely $H(x_j)$. The input data value x_i is replaced by x_j. In practice, we create lookup tables (LUTs) with the SSMI/S value for each channel and the correspondent output SSM/I temperature (reference), which makes this methodology very fast in terms of computing speed.

Because one of the objectives of this study is the continuation of the historical SSM/I–SSMI/S database
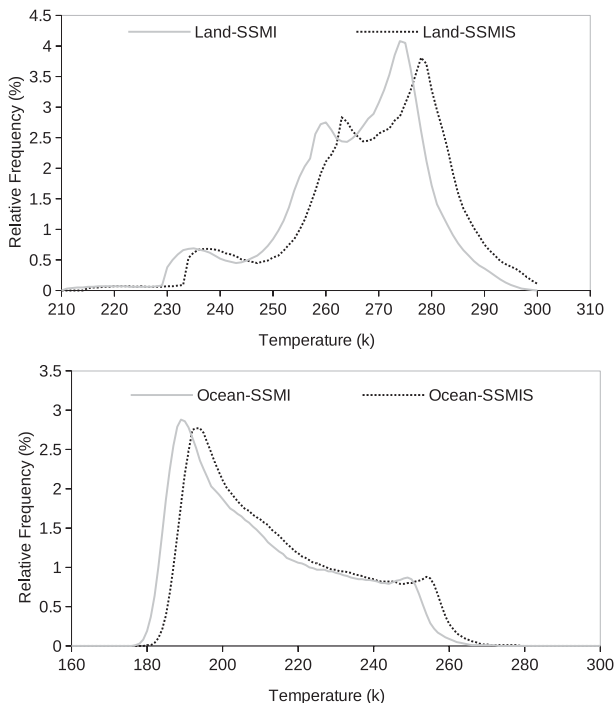
FIG. 2. Probability density function (%) for January 2009 for SSM/I *F-13* (gray solid line) and SSMI/S *F-17* (black dashed line) 22-GHz vertical polarization (top) over land and (bottom) over ocean.

FIG. 3. As in Fig. 2, but for August 2009.

beginning in 1987 and the use of the existing algorithms for hydrological parameters available for SSM/I, the histogram matching approach appears as a suitable scheme to modify SSMI/S temperatures to match with the SSM/I reference.

To achieve this purpose, 7 months between January and July 2009 of ⅓° daily grids for SSM/I *F-13* and SSMI/S *F-17* were chosen to perform this technique. During that period both satellites were flown together with time shift of approximately 1.5 h. Figure 2 shows the probability distribution function (PDF) (in %) for January 2009 for SSM/I *F-13* and SSMI/S *F-17* 22-GHz vertical polarization over ocean and over land, respectively.

It can be seen that both PDFs have a very similar shape but SSMI/S tends to have larger values than SSM/I. This behavior could be due to the fact that there is a time shift between SSM/I and SSMI/S and sensor design.

LUTs for every channel (19-GHz H, 19-GHz V, 22-GHz V, 37-GHz V, 37-GHz H, 91-/85-GHz V, and 91-/85-GHz H) stratified for surface type (land and ocean) were created using global ⅓° global daily grids for January–July 2009 (calibration period). Those LUTs were applied to SSMI/S channels and Fig. 3 shows the PDF for 22-GHz V for August 2009. In this case the solid gray line is SSM/I and the dashed black line is
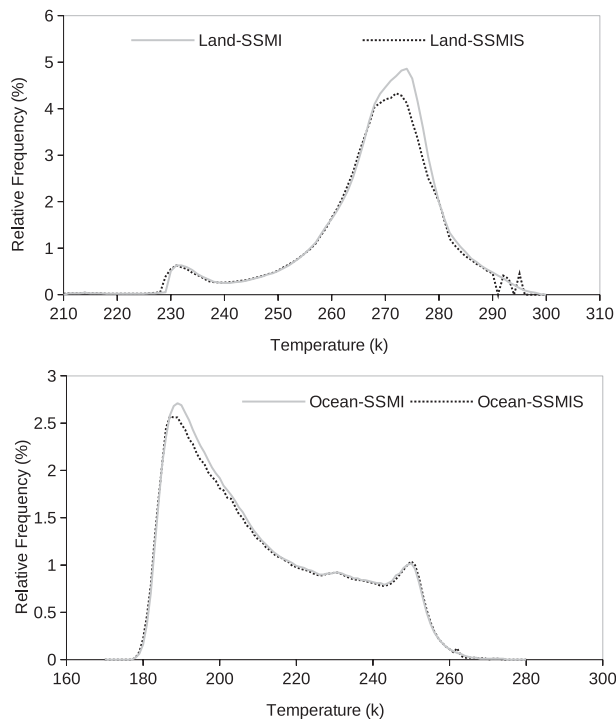
the adjusted SSMI/S value. It is important to notice that August 2009 was not used to create the LUTs, so it can be considered as an independent dataset.

Similar results can be obtained for other channels (not shown). Figure 4 shows the bias between SSMI/S and SSM/I for three different channels (those used for rainfall retrieval—19-GHz V, 22-GHz V, and 91-/85-GHz V) for each temperature during the calibration period. While for low-frequency channels the bias is positive (SSMI/S values are larger than SSM/I values), this behavior is the opposite for high-frequency channels. In this case, this bias is larger (in absolute value) for lower temperatures (especially over land). The depletion of brightness temperature due to the presence of ice is larger for higher frequency (91 GHz) than for 85 GHz. It is also important to notice that this technique is less reliable where few points are present. In the previous figure (Fig. 3—22-GHz V) it can be seen that few pixels are present for temperatures below 175 K over the ocean, so the change of the sign in Fig. 4 (bottom) is not very reliable but it is also not very frequent.

4. The performance of hydrological monthly products

a. Improved QC scheme

The first objective of this paper was the reprocessing of the existing SSM/I database using an improved QC
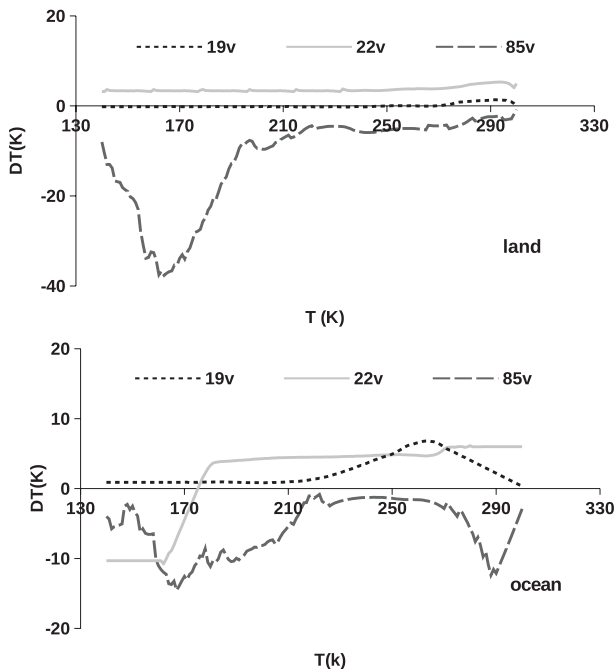
FIG. 4. Bias between SSMI/S and SSM/I for 19-Ghz V (dashed line), 22-GHz V (solid line), and 85-GHz V (long dashed) over (top) land and (bottom) ocean for the calibration period (January–July 2009).
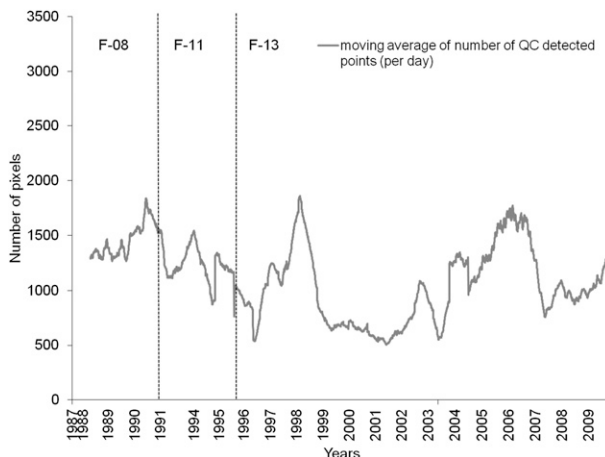

FIG. 5. Moving average of number of daily pixels in the $^1/_3°$ antenna temperature images that were flagged using the QC scheme.

scheme for antenna temperatures for the period 1987–2009 described in section 2c. Figure 5 shows the moving average of number of daily pixels in the $^1/_3°$ antenna temperature images that were excluded using the QC scheme. This mean value for the period 1987–98 is 1100

pixels per image (per day), which represents less than 1% of the total pixels of a given image.

However, this small amount of pixels in the original resolution of $^1/_3°$ can produce an undesirable impact on the monthly products (which is remapped at 2.5° resolution) as is shown in Fig. 6. In this case, it is compared the monthly value of a given product before QC and the same values after QC. If this value changes, this pixel is computed as ''screened by QC scheme.'' This change is expressed as a percentage of total pixels of the global image.

This analysis allows studying the sensibility of each product to erroneous pixels. In the case of precipitation
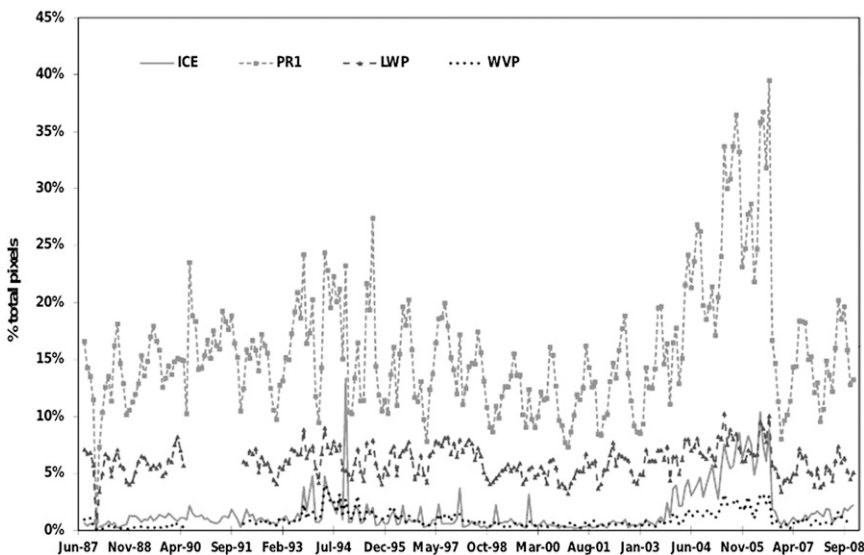

FIG. 6. Percentage of pixels screened by QC scheme on a monthly basis for sea ice (ICE), precipitation (PR1 and PR2, when PR1 is not available), LWP, and WPV.
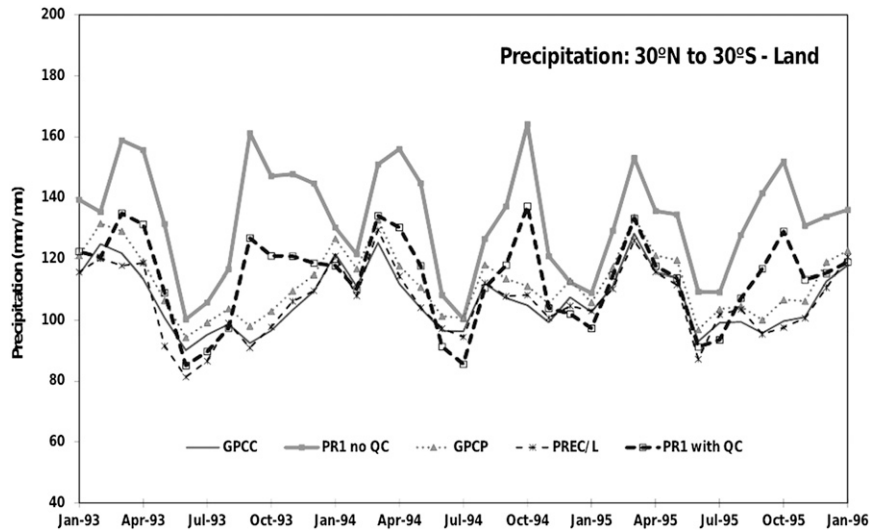
FIG. 7. Precipitation variables for land over tropical regions (30°N–30°S).

(PR1 for the 85.5-GHz algorithm and PR2 for the 37-GHz algorithm), the monthly mean is more affected by bad data (up to 40% of total amount of pixels differs from a non-QC to QC version). PR1 was used for the complete dataset except for the period when *F-08* failed and, in this case, PR2 was used to fill the gap. In the same figure can be observed that WVP is much less affected by bad pixels (below 5%). The case of LWP is less affected than precipitation but the impact is greater than with WVP. It is also important to point out that the maximum in Fig. 6 is coincident with a relative maximum in Fig. 5.

Once the bad data are detected by the QC scheme, it is important to analyze if that screening process has a positive impact on the variable. Figure 7 shows the behavior of precipitation (PR1) for land over tropical regions when it is compared with independent datasets. The period from January 2004–December 2005 was chosen because, according to Fig. 6, a maximum of screened pixels were detected. PR1 with QC (thick dashed black line) is in better agreement with the rest of the independent dataset than the non-QC version (thick solid gray line). In this particular study, three different databases described in section 2a were used to compare with the SSM/I-based retrievals. These are 1) GPCP (Huffman et al. 2009), 2) GPCC (Rudolf 1993), and 3) NOAA's PREC/L (Chen et al. 2002).

b. Transition into SSMI/S era

The second objective of this paper is to evaluate the performance of hydrological monthly products during the SSMI/S era. This era starts in 2006 for midmorning constellation (*F-15* to *F-16* transition) and in late 2009

for early morning constellation (*F-13* to *F-17* transition). As mentioned before, the latter constellation is particularly important because it is the reference for rainfall retrieval over land for GPCP V2 (among other users) because it presents the longest data record back to 1987. In the next paragraphs we intend to address a comparison between SSM/I and SSMI/S for three different hydrological variables during the period where they were flying together (January–November 2009): rainfall rate (PR1), WVP, and LWP. Figure 8 shows the histogram for light and high rain rates for August 2009 over land and ocean. This data could be considered as independent because this month was not used to create the LUTs. During this month (a similar behavior is observed in other months) the histograms are pretty similar for light and medium rates (the most frequent) and SSMI/S tends to overestimate the rainfall for high rain rates (the less-frequent events).

However, when the zonal mean for the same month is shown (Fig. 9), the differences are very small for all latitudes over ocean, while over land the overestimation of high rain rates for SSMI/S is reflected in a slight overestimation of maximum values in the Northern Hemisphere (summertime).

A similar analysis was done with LWP and WVP over the ocean (those variables are retrieved only over ocean). Figure 10 shows the behavior of both variables (LWP on the right and WVP on the left) where a maximum near the equator is observed in both variables and a secondary maximum for LWP is also observed at 40°S, coincident with the most active storm track region in wintertime over Southern Hemisphere. In the case of LWP, SSMI/S retrievals tend to overestimate the maximum located in
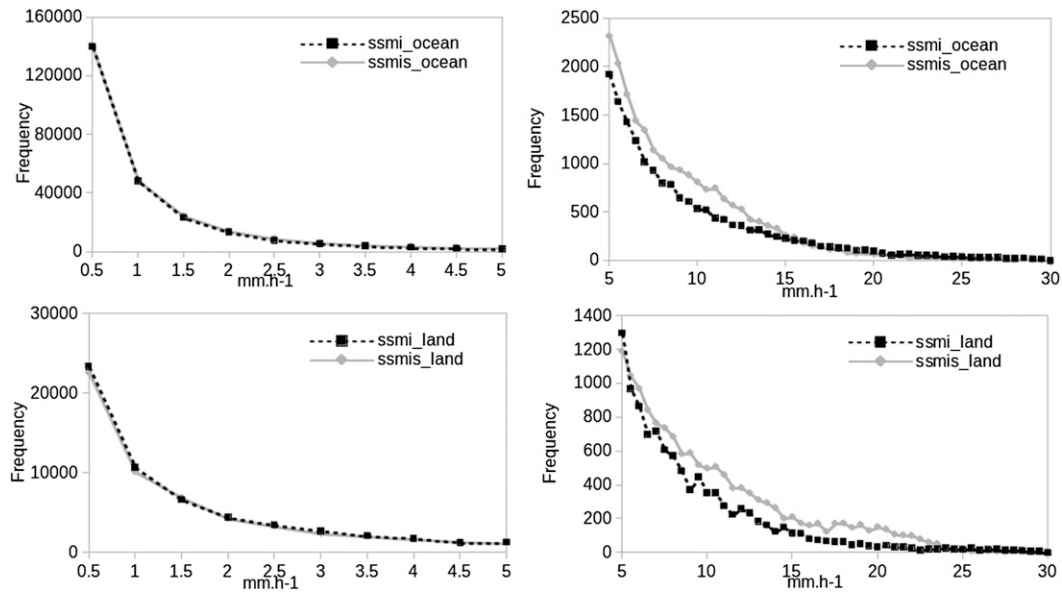
FIG. 8. Histogram for (left) light and (right) high rain rates over (top) ocean and (bottom) land for August 2009. Dashed black curve is for SSM/I *F-13* and gray solid curve is for SSMI/S *F-17*.

the tropics while for WVP no noticeable bias is observed for all latitudes.

Figure 11 shows the monthly rainfall bias (expressed in terms of percentage of monthly mean) for global, ocean, and land surfaces for the period January–November 2009 when both satellites were flying together. The observed bias is below 10% for all analyzed months with the exception of April 2009. The bottom panel shows the frequency bias (expressed in terms of percentage of mean number of rainy pixels for a given month) behavior for the period January–November 2009. The observed values are very small and negative (less than 1% in absolute value), suggesting that the number of pixels with rainfall for both satellites is very similar.

A similar behavior could be observed for LWP and WVP. In the case of LWP, the difference between SSM/I and SSMI/S retrievals is below 4% of the mean value (Fig. 12, black bars) for all months with the exception of April 2009, while for WVP (Fig. 12, gray lines) the bias is below 2%, suggesting that the sensibility for this variable is smaller than for LWP and PR1.

To assess the performance of PR1 time series during the transition period, the merged dataset (*F-13* before January 2009 and *F-17* after that) was compared with the GPCC monitoring product, version 4 (Rudolf 1993) for the region 60°N–60°S over land. This global land-based monthly rainfall product based upon surface rain gauges (version 4 is only available from 2007) offers a completely independent database to evaluate the behavior of global precipitation during the short period where

only SSMI/S is available (2009–11) over land. Five years of monthly data (January 2007–December 2011) were used to assess the behavior of PR1 during the transition between SSM/I *F-13* and SSMI/S *F-17*.
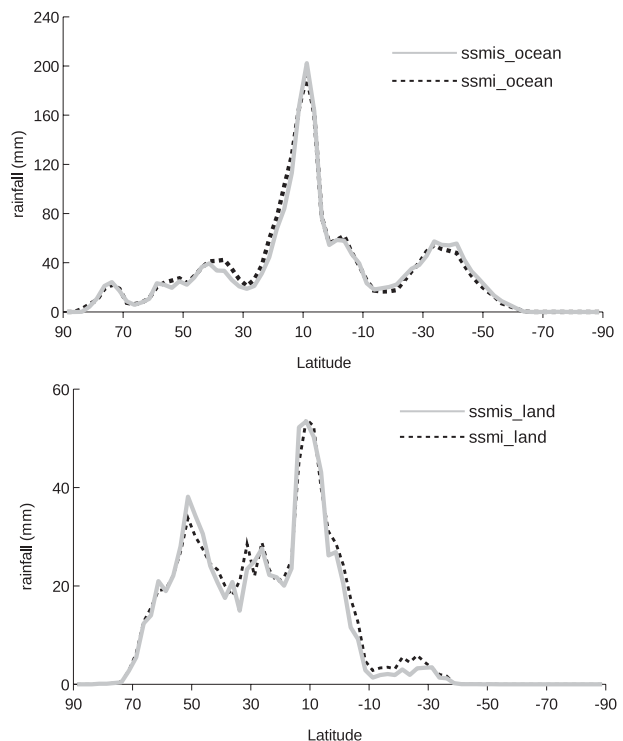

FIG. 9. Zonal mean for monthly rainfall in August 2009 for *F-17* (SSMI/S, solid gray line) and *F-13* (SSM/I, dashed black line) over (top) ocean and (bottom) land.
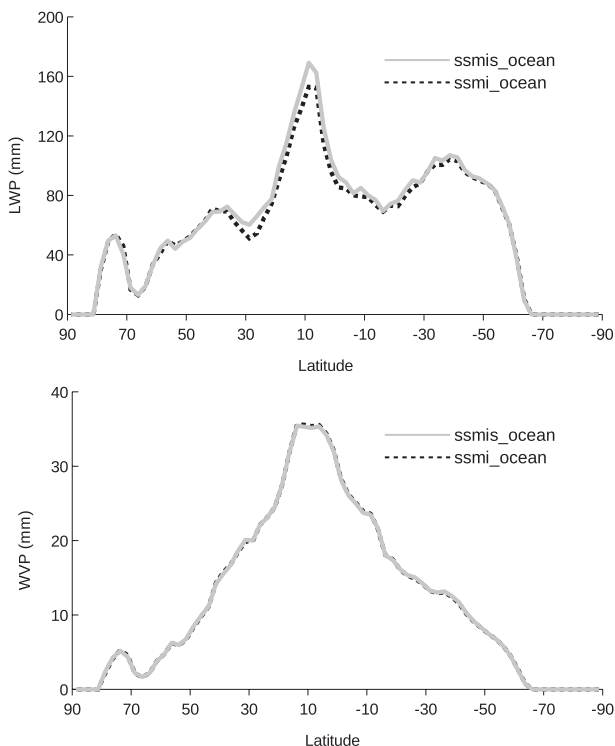
FIG. 10. Zonal mean for monthly (top) LWP and (bottom) WVP during August 2009 for *F-17* (SSMI/S, solid gray line) and *F-13* (SSM/I, dashed black line).
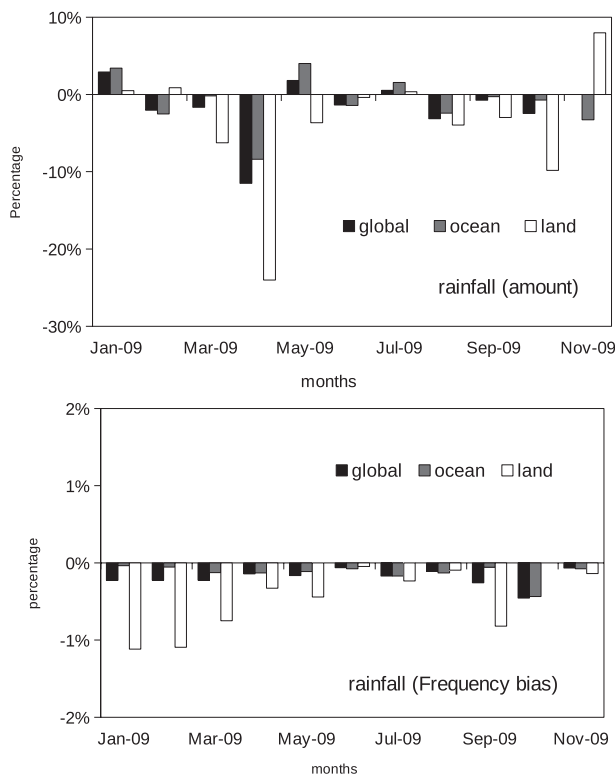

FIG. 11. (top) Monthly rainfall bias (in terms of percentage of the mean value) for global (black bars), ocean (dark gray bars), and land surfaces (white bars) for the period January–November 2009. Negative values mean larger SSMI/S retrievals. (bottom) As above, but for frequency bias.

When the 5-yr period is considered, the quasi-global average for GPCC and PR1 is 62.8 mm month^{-1} for both datasets with a standard deviation of 6.8 and 5.8 mm, respectively, so no difference in the mean value is observed. In case of considering two different periods, 2007/08 for SSM/I and 2009/11 for SSMI/S, the mean values are 60.9 and 63.0 mm month^{-1} for the SSM/I period for PR1 and GPCC, respectively, while 64.0 and 62.7 mm month^{-1} is observed for the SSMI/S period with a bias of 2.9 mm month^{-1} (less than 5%) for SSMI–SSMI/S comparison. This value is consistent with the assessment done during the period when *F-13* and *F-17* were flying together. Figure 13 shows the time series for SSM/I–SSMI/S merged series and GPCC for the mentioned period. It is important to notice that rain gauge observations offer a direct but randomly distributed measurements of rainfall, while the SSM/I–SSMI/S merged product (*F-13*, *F-17*) is based on an indirect methodology for retrieving rainfall and only has two daily measurements (one ascending and one descending) for every point of the considered region (60°N–60°S).

5. Summary and conclusions

The two objectives of this research—the reprocessing of the existing SSM/I database using an improved QC

scheme for antenna temperatures for the entire period (1987–2011) and the continuation in monitoring and retrieving of atmospheric and surface parameters using SSMI/S measurements—have been reached. The early stages of *F-08* satellite from August 1987 to December 1991 were reprocessed and the QC scheme (with restrictions due to the failure of 85 GHz during June
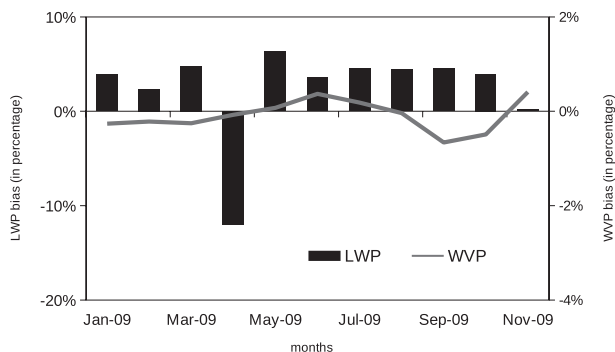

FIG. 12. Monthly bias for LWP (black bars) and WVP (dark gray lines) over the ocean for the period January–November 2009. Positive values mean larger SSMI/S retrievals.
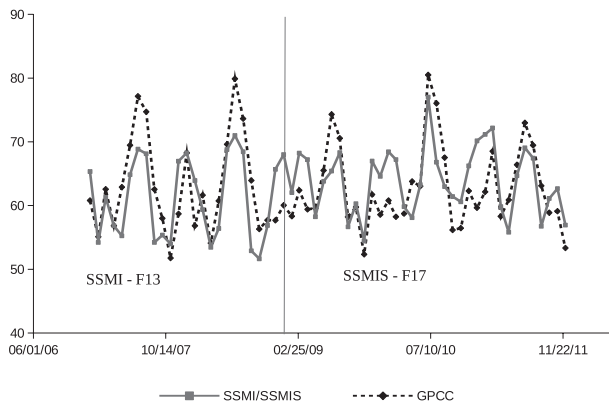
Fig. 13. Time series for SSMI–SSMI/S merged database (solid gray lines) and GPCC (dashed black lines) for the period 2007–11. The solid vertical line represents the merging date (January 2009) between SSM/I *F-13* and SSMI/S *F-17*.

1990–December 1991) was applied. The entire data record of $\frac{1}{3}°$ latitude $\times$ $\frac{1}{3}°$ longitude linear daily grids for the ascending and descending for all SSM/I sensors (*F-08*, *F-10*, *F-11*, *F-13*, *F-14*, and *F-15*) starting in 1987 to December 2011 are reprocessed and quality controlled for further use in any application.

For this particular research, some hydrological monthly products like rain rate, liquid water path, and total precipitable water were evaluated in order to get an assessment on how the flagged pixels detected in the QC scheme can impact on the retrieved value. While less than 1% of the total pixels of each image were flagged, up to 40% of the pixels could differ on monthly rain rate when a non-QC or QC version of the database is used. Because this assessment depends on the algorithm, other monthly products, like WVP, are less sensible to erroneous pixels in the global monthly scale (less than 5%). In general terms, as it was observed in previous studies (i.e., Vila et al. 2010), a positive impact is observed when QC is applied.

The second objective of this study is the continuation of the historical database beginning in 1987 and the use of the existing algorithms for hydrological parameters available for SSM/I. The histogram matching approach worked very well to modify SSMI/S temperatures to match with the SSM/I reference. A comparison between SSM/I *F-13* and SSMI/S *F-17* retrievals during the period January 2009–October 2009 for rainfall rate, total precipitable water, and liquid water path were performed to evaluate this approach. SSM/I *F-13* and SSMI/S *F-17* retrievals are particularly important because they are the reference for rainfall retrieval over land for GPCP V2 among other users. The results obtained

show a very good agreement between SSM/I and SSMI/S retrievals for all analyzed variables, suggesting that the LUTs applied during the coincident period could be applied for the further SSMI/S period (2010 and beyond).

REFERENCES

Alihouse, J. C., S. Snyder, J. Vongsathorn, and R. Ferraro, 1990: Determination of total precipitable water from the SSM/I. *IEEE Trans. Geosci. Remote Sens.,* **28,** 811–816.

Chen, M., P. Xie, J. E. Janowiak, and P. A. Arkin, 2002: Global land precipitation: A 50-yr monthly analysis based on gauge observations. *J. Hydrometeor.,* **3,** 249–266.

Colton, M., and G. Poe, 1994: Shared Processing Program, Defense Meteorological Satellite Program, Special Sensor Microwave/Imager Algorithm Symposium, 8–10 June 1993. *Bull. Amer. Meteor. Soc.,* **75,** 1663–1669.

Ferraro, R. R., 1997: Special Sensor Microwave Imager derived global rainfall estimates for climatological applications. *J. Geophys. Res.,* **102** (D14), 16 715–16 735.

——, N. C. Grody, F. Weng, and A. Basist, 1996: An eight-year (1987–1994) time series of rainfall, clouds, water vapor, snow cover, and sea ice derived from SSM/I measurements. *Bull. Amer. Meteor. Soc.,* **77,** 891–905.

Gonzalez, R., and R. E. Woods, 2002: *Digital Image Processing.* 2nd ed. Prentice Hall, 793 pp.

Grody, N. C., 1991: Classification of snow cover and precipitation using the Special Sensor Microwave Imager. *J. Geophys. Res.,* **96** (D4), 7423–7435.

Huffman, G. J., R. F. Adler, D. T. Bolvin, and G. Gu, 2009: Improving the global precipitation record: GPCP version 2.1. *Geophys. Res. Lett.,* **36,** L17808, doi:10.1029/2009GL040000.

Poe, G. A., K. Germain, J. Bobak, S. Swadley, J. Wessel, B. Thomas, J. Wang, and B. Burns, 2001: DMSP calibration/validation plan for the Special Sensor Microwave Imager Sounder (SSMIS). Naval Research Laboratory, 32 pp.

Rudolf, B., 1993: Management and analysis of precipitation data on a routine basis. *Proc. Int. WMO/IAHS/ETH Symp. on Precipitation and Evaporation,* Vol. 1, Bratislava, Slovakia, Slovak Hydrometeorological Institute, 69–76.

Vila, D., R. Ferraro, and R. Joyce, 2007: Evaluation and improvement of AMSU precipitation retrievals. *J. Geophys. Res.,* **112,** D20119, doi:10.1029/2007JD008617.

——, ——, H. Semunegus, 2010: Improved global rainfall retrieval using the Special Sensor Microwave Imager (SSM/I). *J. Appl. Meteor. Climatol.,* **49,** 1032–1043.

Weng, F., and N. C. Grody, 1994: Retrieval of cloud liquid water using the Special Sensor Microwave Imager (SSM/I). *J. Geophys. Res.,* **99** (D12), 25 535–25 551.